2018 IEEE Conference on Decision and Control (CDC)
Miami Beach, FL, USA, Dec. 17-19, 2018

Estimation of Multiple Flexibilities of an Articulated System Using Inertial Measurements

Matthieu Vigne*† , Antonio El Khoury*, Matthieu Masselin *, Florent Di Meglio† and Nicolas Petit†
*Control-Command team, Wandercraft, Paris, France
Email: matthieu.vigne@mines-paristech.fr
†Centre Automatique et Systèmes, MINES ParisTech, PSL Research University, France

***Abstract*— For many articulated systems (i.e. systems composed of several mechanically connected objects), the assumption of full rigidity is only a mere approximation. The various flexibilities of the structure, if not accounted for, all hinder the positioning ability of the device, by generating biases in the estimations determined from rigid models. In this paper, we propose a sensor-based methodology for estimating the flexibilities of an open kinematic chain. To estimate the real position and orientation of the elements of the system, we reconcile data from Inertial Measurement Units (IMU) with the kinematics of the rigid system. We show that, under a model of punctual, spring-like deformations, this methodology allows one to observe all the deformations, if one IMU is installed downstream of each deformation in the chain. We design and test such an observer in simulation and on an exoskeleton, where it proved a suitable way of estimating the position of the flying foot. Experimental results, validated against a motion capture device, demonstrate the ability of this observer to fully capture the dynamics induced by these flexibilities.**

I. Introduction

Estimating the position of an open kinematic chain is a general problem of practical importance in robotics. It represents a central question to enable precise motion of a manipulator [1] [2], or to make a legged robot walk [3] [4]. Apart from the positioning of each actuator, the overall kinematics of the structure is a key element to determine the position of the various elements of the chain. While motor information (rotary encoders) gives these positions in a straightforward, unambiguous manner for a completely rigid structure, in practice, some flexibilities may be present at weaker points in the structure. The weaknesses are often a side-effect of design constraints, such as mass or size limitations. They may also be a resolute design choice: as is well documented, see e.g. [5], compliance protects the structure from impacts, may be used to improve ground contact, and creates additional mobility to the system. In this paper, we study the estimation of flexibilities. We distinguish between:

- joints instrumented with encoders (actuated or not), which we simply call joints.
- degrees of freedom accounting for these deformations, which we call flexibilities. These flexibilities are assumed to be punctual, 3D rotations, with a spring-like behavior.

The main objective of this paper is to estimate their angle based on IMUs.

The motivation for such work arises from the study of the exoskeleton depicted in Figure 1, which has a flexible behavior. This fact was clearly evidenced by motion capture experiments showing a mismatch between the measured absolute position measurements and the rigid body model:

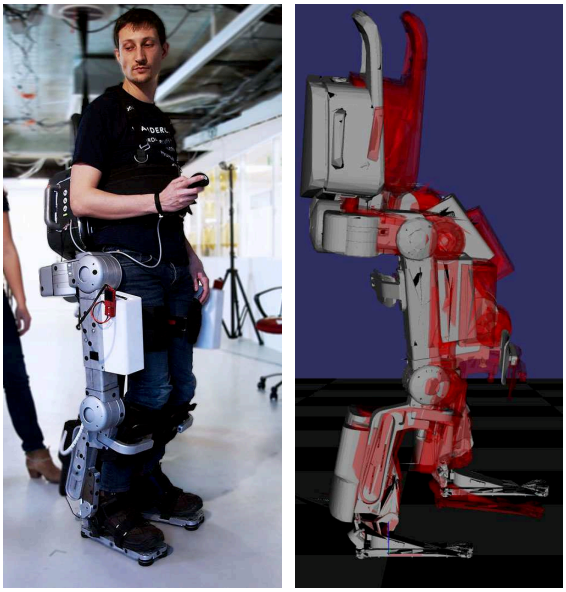

Fig. 1. Picture of Atalante™, an exoskeleton developed by Wandercraft. On the right, CAD reconstruction under the assumption of full rigidity (gray), and real deformed configuration (red), as measured by a motion capture device.

in Figure 1, the real robot state (in red) does not match the predicted rigid states model (in gray): the only possible source of error are the flexibilities at several points in the structure. An objective of practical importance is to estimate the real position of the flying foot, which is the end effector of the chain, taking this effect into account.

Using inertial information to reconstruct the attitude of an object has become a popular trend [6] [7] [8] [9], with the advent of MEMS sensors which can easily be placed on a device such as the exoskeleton of Figure 1. Various kinds of filters, like Kalman or complementary filters, have been used to reconcile accelerometers and gyroscopes (and sometimes magnetometers) measurements (see for example [7] and references therein). For kinematically constrained systems, constraints may be put into the formulation of the attitude observer (see for example [10] or [11]). Without any specific assumption on the kinematics of the system, such filters implicitly consider that, on average, the accelerometer gives the direction of gravity. This is not the case for fast-moving systems, such as a robotic platform. However, when kinematic information is available (e.g. through encoder information), it could be subtracted from inertial sensor readings, providing (theoretically exact) cancellation of the disturbances, to give a better estimate of the true pose of the system [12], [13], [14]. Knowing where the deformation

takes place can be introduced as a kinematic constraint (see for example work done on HRP-2, a humanoid with flexible ankles, in [15] and [16]). Moreover, when the rotation being estimated stems from structural flexibility but is not directly measured, a dynamic model can also be added, such as in [17]. All these examples however consider that there is only one unknown rotation to be observed: to our knowledge, the presence of several deformations inside an otherwise rigid structure has not been addressed. This is precisely the topic under consideration in this article: we consider n IMUs to reconstruct n flexibilities.

The main contribution of this paper is a methodology for estimating the flexibilities distributed along an open kinematic chain of arbitrary length using the mechanical description of each object in the articulated system and measurements of strapdown IMUs. In accordance with our definition of flexibilities given above, we formulate this estimation problem by assuming that, overall, the structure is composed of rigid bodies and instrumented joints, apart from specific points where unmeasured rotations occur. At these points, the deformation is modeled by a spring. For each deformation, an IMU is placed in one of the downstream bodies of the chain, to observe this rotation. Using this sensor, information about the state of the joints, and the resulting dynamical model, we estimate the position of each element of the chain. We show that the full state is observable. Then, an observer is implemented (an EKF), and simulation results are proposed to assess its performance. Finally, experimental results obtained using a motion capture device as reference stress the accuracy of the reconstruction.

The paper is organized as follows: in Section II, we present the class of system under consideration, and a model of flexibilities. In Section III, the state dynamics of the system is presented. This state is then shown to be observable in Section IV. Finally, Section V presents simulation and experimental results.

II. Problem Parametrization

Notations: throughout this paper, the following notations are used: given two orthonormal frames of reference A and B, and a point c, we write ${}^A\boldsymbol{p}_c$ the coordinates of c in A, ${}^B R_A$ the rotation from frame A to frame B (such that if A and B have the same origin, ${}^B\boldsymbol{p}_c = {}^B R_A\, {}^A\boldsymbol{p}_c$). The variable ${}^B\boldsymbol{\omega}_A$ is the angular velocity vector of frame A relative to frame B, expressed in frame B. Finally, $[.]_\times$ is the operator that associates to a vector x the skew-symmetric matrix such that $[x]_\times y = x \times y$, for all y.

Consider a n_b-bodies system forming an open kinematic chain (for example, a robotic arm or a humanoid robot in single support). To describe the position of the flexibilities in the system, we gather the rigid bodies into $n+1$ sets S_i, $i \in [0, n]$, each set having only measured internal dynamics. S_0, the set supporting the open kinematic chain, is here assumed to be linked with the world frame (this is the case if the system is a walking robot in single support, with one foot touching the ground)[1]. Let O_i be the point linking S_{i-1} with S_i, i.e. the point where the flexibility takes place. To represent the flexibilities, we define C_i a frame centered in O_i, rotated from the world frame by the total flexibility applied to the set S_i. Thus, ${}^{C_{i-1}}R_{C_i}$ represents the rotation of the ith flexibility, while ${}^W R_{C_i}$ gives the combined effect of the first ith flexibilities. Note that the definition of C_i is independent of joint motion, but only reflects the total flexibility at a certain point. For convenience, we define $C_0 = W$. Figure 2 gives a representation of these frames. Table I gives a summary of these notations and those defined hereafter.

[1]Note that, as long as the kinematics of the (possibly non-Galilean) frame linked to S_0 is known, the results in this article may be applied (the only difference would be the addition of a known fictitious force term in the forthcoming equation (7)).

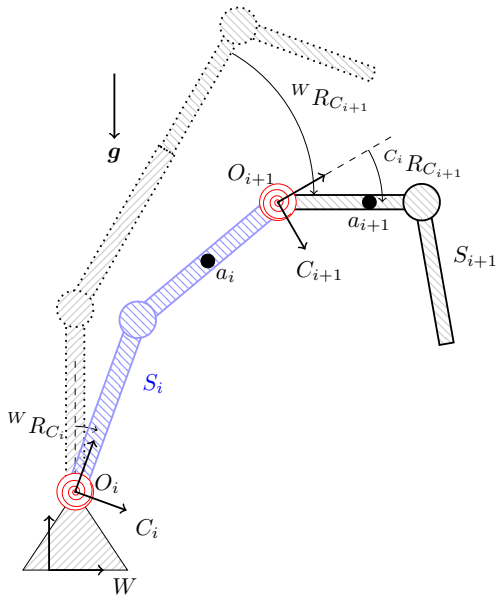

Fig. 2. Representation of two body sets S_i and S_{i+1}. The circles represent system joints, and the red spirals flexibilities. The dots a_i and a_{i+1} show the location of the IMU in each set. The dotted set shows the configuration of the chain in the absence of all deformations.

The general problem under consideration is stated below.

Problem 1: Given a set of IMUs and actuator measurements, estimate the current flexible state of the system, that is, determine all the rotation matrices ${}^{C_{i-1}}R_{C_i}$ and the corresponding velocities ${}^{C_{i-1}}\boldsymbol{\omega}_{C_i}$.

To solve this problem, we make the following additional assumptions:

Assumption 1: The deformations of the system due to the flexibilities remain small, and can be modeled as the decoupled deformation of linear torsion springs. More specifically, calling $\boldsymbol{\tau}_i$ the torque generated on S_i by S_{i-1}, in frame C_i, we have

$$\boldsymbol{\tau}_i \triangleq -K_i\, {}^{C_{i-1}}\boldsymbol{\Omega}_{C_i} \tag{1}$$

where ${}^{C_{i-1}}\boldsymbol{\Omega}_{C_i}$ is the rotation vector associated to ${}^{C_{i-1}}R_{C_i}$ through the exponential map [18]

$${}^{C_{i-1}}R_{C_i} = \exp\left([{}^{C_{i-1}}\boldsymbol{\Omega}_{C_i}]_\times\right)$$

and K_i is a positive-definite symmetrical matrix, representing the stiffness of the joint.

Assumption 2: The dimensions, mass and inertia of all the bodies of the system are known. Additionally, the joint configuration of the system is measured. We call $\boldsymbol{q}_j$ this generalized position, $\boldsymbol{\alpha}_j$ and $\dot{\boldsymbol{\alpha}}_j$ the corresponding velocity and acceleration

Note that, for simple revolute joints, $\boldsymbol{\alpha}_j$ is simply the derivative of $\boldsymbol{q}_j$, but generically this is not always the case,

as position and velocity may be represented by different coordinates, see [19, Chapter 4]. In this case, we shall write

$$\dot{\boldsymbol{q}}_j = Q_j(\boldsymbol{q}_j)\boldsymbol{\alpha}_j \tag{2}$$

Assumption 3: Each set S_i, $i = [1, n]$, is equipped with one IMU, consisting of a 3-axis accelerometer and a 3-axis gyroscope (we thus place as many IMUs as flexibilities, i.e. n). We consider the position and orientation of the IMUs in the body frame to be known. In the theoretical study, we do not consider gyroscope bias, assuming it has been previously debiased by, e.g., the filter implemented in [7].

We define $\boldsymbol{x}$, the state to estimate, and $\boldsymbol{u}$, the vector of known inputs, as:

$$\boldsymbol{x} \triangleq \begin{pmatrix} q_1 \\ \dots \\ q_n \\ \boldsymbol{\omega}_1 \\ \dots \\ \boldsymbol{\omega}_n \end{pmatrix} \triangleq \begin{pmatrix} \boldsymbol{q}_f \\ \boldsymbol{\alpha}_f \end{pmatrix} \qquad \boldsymbol{u} \triangleq \begin{pmatrix} \boldsymbol{q}_j \\ \boldsymbol{\alpha}_j \\ \dot{\boldsymbol{\alpha}}_j \end{pmatrix} \tag{3}$$

where q_i is a quaternion representing the rotation matrix ${}^{C_{i-1}}R_{C_i}$ and $\boldsymbol{\omega}_i = {}^{C_i}R_{C_{i-1}}\,{}^{C_{i-1}}\boldsymbol{\omega}_{C_i}$ is the rotation velocity of set S_i relative to S_{i-1}, expressed in C_i. The variables $\boldsymbol{q}_f$ and $\boldsymbol{\alpha}_f$ are the quaternion and angular velocity parts of $\boldsymbol{x}$ respectively. Note that there is a one-to-one mapping between $\boldsymbol{x}$ and the vector $({}^{W}R_{C_1} \dots {}^{W}R_{C_n}\,{}^{W}\boldsymbol{\omega}_{C_1} \dots {}^{W}\boldsymbol{\omega}_{C_n})$ through the following equations

$$\begin{cases} {}^{W}R_{C_i} = {}^{W}R_{C_1}\,{}^{C_1}R_{C_2} \dots {}^{C_{i-1}}R_{C_i} \\ {}^{W}\boldsymbol{\omega}_{C_i} = \sum_{k=0}^{i} {}^{W}R_{C_{k-1}}\boldsymbol{\omega}_k \end{cases} \tag{4}$$

To solve Problem 1, we prove in Section IV the result given below (Theorem 1).

Definition 1: [20, Definition 2.4.1] The system defined by

$$\begin{cases} \dot{\boldsymbol{x}} = f(\boldsymbol{x}, \boldsymbol{u}) \\ \boldsymbol{y} = h(\boldsymbol{x}, \boldsymbol{u}) \end{cases} \tag{5}$$

is E-uniformly observable if, for any $T > 0$ and any input $\boldsymbol{u} : [0, T] \mapsto E$, $\boldsymbol{u}$ distinguishes every pair of initial state.

Theorem 1: Under Assumption 1-3, the state $\boldsymbol{x}$ defined in (3) is E-uniformly observable.

An interesting feature of Theorem 1 is that the observable state x includes the full 3D rotation of the IMU. The observability of the yaw deformation, in particular, is made possible by the modeling of the deformation as a spring, which alleviates the traditional need for an additional absolute measurement such as a magnetometer. Before giving the proof of this theorem in Section IV, we derive in the next section the state dynamics f and output equation h.

III. State and measurements dynamics

A. Derivation of system dynamics f

The kinematics of the system consists of the motion at the joints, described by $\boldsymbol{q}_j$, and the motion of the flexibilities, $\boldsymbol{q}_f$. Thus we define the full generalized position and velocity vector of the system as:

$$\boldsymbol{q} \triangleq \begin{pmatrix} \boldsymbol{q}_j \\ \boldsymbol{q}_f \end{pmatrix} \qquad \boldsymbol{\alpha} \triangleq \begin{pmatrix} \boldsymbol{\alpha}_j \\ \boldsymbol{\alpha}_f \end{pmatrix} \tag{6}$$

TABLE I
Frequently used notations

${}^{A}\boldsymbol{p}_c$	Position of point c in frame A.
${}^{B}R_A$	Rotation from frame A to B.
${}^{B}\boldsymbol{\omega}_A$	Angular velocity of A relative to frame B, in frame B.
$[\boldsymbol{x}]_\times$	Skew-symmetric matrix such that $[\boldsymbol{x}]_\times \boldsymbol{y} = \boldsymbol{x} \times \boldsymbol{y}$
S_i for $i \in [0, n]$	Sets of bodies of the system, internally articulated only with measured joints.
O_i for $i \in [1, n]$	The point of junction between S_{i-1} and S_i were a flexibility is placed.
C_i for $i \in [1, n]$	Frame associated with the deformation at O_i, representing the flexibility.
W	The world frame, also noted C_0.
I_i for $i \in [0, n]$	Frame associated to the IMU placed in S_i.
a_i for $i \in [0, n]$	Localization of the IMU placed in S_i.
q_i for $i \in [1, n]$	Quaternion representation of ${}^{C_{i-1}}R_{C_i}$
$\boldsymbol{\omega}_i$ for $i \in [1, n]$	Relative angular velocity of the flexibility: $\boldsymbol{\omega}_i = {}^{C_i}R_{C_{i-1}}\,{}^{C_{i-1}}\boldsymbol{\omega}_{C_i}$.
$\boldsymbol{q}_f$	Generalized position vector of the flexibilities.
$\boldsymbol{\alpha}_f$	Generalized velocity vector of the flexibilities.
$\boldsymbol{q}_j$	Generalized position vector of the joints.
$\boldsymbol{\alpha}_j$	Generalized velocity vector of the joints.

The dynamics of an open kinematic chain of rigid bodies is a topic that has already been thoroughly studied (see for example [19] for a comprehensive analysis of such problem). Taking the notations of [19, eq. 3.5], the inverse dynamics of this system can be generically written as:

$$H(\boldsymbol{q})\dot{\boldsymbol{\alpha}} + \boldsymbol{C}(\boldsymbol{q}, \boldsymbol{\alpha}) = \boldsymbol{\tau} \tag{7}$$

where $H(\boldsymbol{q})$ is the generalized symmetric inertia matrix of the system, $\boldsymbol{C}(\boldsymbol{q}, \boldsymbol{\alpha})$ is the generalized bias force (taking into account inertial forces and the effect of gravity), and $\boldsymbol{\tau}$ is the vector of generalized external forces acting on the joints. To solve (7) for $\dot{\boldsymbol{\alpha}}_f$, we split the rigid and flexible parts of this equation as:

$$\begin{pmatrix} H_j(\boldsymbol{q}) & H_{jf}^T(\boldsymbol{q}) \\ H_{jf}(\boldsymbol{q}) & H_f(\boldsymbol{q}) \end{pmatrix} \begin{pmatrix} \dot{\boldsymbol{\alpha}}_j \\ \dot{\boldsymbol{\alpha}}_f \end{pmatrix} = \begin{pmatrix} \boldsymbol{\tau}_j - \boldsymbol{C}_j(\boldsymbol{q}, \boldsymbol{\alpha}) \\ \boldsymbol{\tau}_f(\boldsymbol{q}_f) - \boldsymbol{C}_f(\boldsymbol{q}, \boldsymbol{\alpha}) \end{pmatrix} \tag{8}$$

where $\boldsymbol{\tau}_f$, the torque applied to the flexible joints, is described by (1), and is only a function of $\boldsymbol{q}_f$.

The second line of this equation yields:

$$\dot{\boldsymbol{\alpha}}_f = H_f^{-1}(\boldsymbol{q}) \left(\boldsymbol{\tau}_f(\boldsymbol{q}_f) - \boldsymbol{C}_f(\boldsymbol{q}, \boldsymbol{\alpha}) - H_{rf}(\boldsymbol{q})\dot{\boldsymbol{\alpha}}_j\right) \tag{9}$$

Summing up (9) and the relation between the derivative of the quaternions and $\boldsymbol{\alpha}_f$ yields

$$\dot{\boldsymbol{x}} = \begin{pmatrix} Q_f(\boldsymbol{q}_f)\boldsymbol{\alpha}_f \\ H_f^{-1}(\boldsymbol{q}) \left(\boldsymbol{\tau}_f(\boldsymbol{q}_f) - \boldsymbol{C}_f(\boldsymbol{q}, \boldsymbol{\alpha}) - H_{rf}(\boldsymbol{q})\dot{\boldsymbol{\alpha}}_j\right) \end{pmatrix} \tag{10}$$

where $Q_f(\boldsymbol{q}_f)$ is given by [19, eq. 4.13]. This relationship is indeed of the desired form (5).

B. Derivation of measurement equation h

Let $i \in [1, n]$. We here derive the equations defining the measurement from the IMU in the set S_i. Let a_i be the center point of the sensor, and I_i the sensor measurement frame. The gyroscope measures the body angular velocity, whereas the accelerometer measures its specific acceleration. Both do

so in their respective sensor frame, which we both take equal to I_i for simplicity of notation. Thus, we have:

$$\begin{cases} \boldsymbol{y}_a = {}^{I_i}R_W({}^W\ddot{\boldsymbol{p}}_{a_i} - {}^W\boldsymbol{g}) \\ \boldsymbol{y}_g = {}^{I_i}R_W\,{}^W\boldsymbol{\omega}_S \end{cases} \tag{11}$$

where $\boldsymbol{y}_a$ is the accelerometer output, $\boldsymbol{y}_g$ the gyroscope output, and ${}^W\boldsymbol{g}$ the gravity vector.

To express this equation as a function of $\boldsymbol{x}$ and $\boldsymbol{u}$ only, we split the motion of the IMU in the world as the combination of the motion of the IMU in C_i (which is entirely defined by $\boldsymbol{u}$), and the motion of C_i in the world, which depends both on the flexible and the rigid dynamics:

$$\begin{aligned} \boldsymbol{y}_g &= {}^{I_i}R_W({}^W\boldsymbol{\omega}_{C_i} + {}^WR_{C_i}\,{}^{C_i}\boldsymbol{\omega}_S(\boldsymbol{q}_j, \boldsymbol{\alpha}_j)) \\ &= {}^{I_i}R_{C_i}(\boldsymbol{q}_j)({}^{C_i}R_W\,{}^W\boldsymbol{\omega}_{C_i} + {}^{C_i}\boldsymbol{\omega}_S(\boldsymbol{q}_j, \boldsymbol{\alpha}_j)) \end{aligned} \tag{12}$$

From (4), ${}^{C_i}R_W$ and ${}^W\boldsymbol{\omega}_{C_i}$ are functions of $\boldsymbol{x}$ only. Thus, (12) gives the expression of the gyroscope measurements as a function of $\boldsymbol{x}$ and $\boldsymbol{u}$. Similarly, the linear acceleration of the sensor can be rewritten

$$\begin{aligned} {}^W\ddot{\boldsymbol{p}}_{a_i} = {}&{}^WR_{C_i}\,{}^{C_i}\ddot{\boldsymbol{p}}_{a_i}(\boldsymbol{q}_j, \boldsymbol{\alpha}_j, \dot{\boldsymbol{\alpha}}_j) \\ &+ {}^W\ddot{\boldsymbol{p}}_{O_i} \\ &+ [{}^W\dot{\boldsymbol{\omega}}_{C_i}]_\times\,{}^WR_{C_i}\,{}^{C_i}\boldsymbol{p}_{a_i}(\boldsymbol{q}_j) \\ &+ [{}^W\boldsymbol{\omega}_{C_i}]_\times^2\,{}^WR_{C_i}\,{}^{C_i}\boldsymbol{p}_{a_i}(\boldsymbol{q}_j) \\ &+ 2[{}^W\boldsymbol{\omega}_{C_i}]_\times\,{}^WR_{C_i}\,{}^{C_i}\dot{\boldsymbol{p}}_{a_i}(\boldsymbol{q}_j, \boldsymbol{\alpha}_j) \end{aligned} \tag{13}$$

The acceleration of the origin of the frame ${}^W\ddot{\boldsymbol{p}}_{O_i}$ can be computed by chaining changes of referential for O_i through C_{i-1}, C_{i-2}, ..., $C_0 = W$ as follows

$$\begin{aligned} {}^W\ddot{\boldsymbol{p}}_{O_i} = \sum_{k=1}^{i}\Big[{}&{}^WR_{C_{k-1}}\,{}^{C_{k-1}}\ddot{\boldsymbol{p}}_{O_k}(\boldsymbol{q}_j, \boldsymbol{\alpha}_j, \dot{\boldsymbol{\alpha}}_j) \\ &+ [{}^W\dot{\boldsymbol{\omega}}_{C_{k-1}}]_\times\,{}^WR_{C_{k-1}}\,{}^{O_{k-1}}\boldsymbol{p}_{C_k}(\boldsymbol{q}_j) \\ &+ [{}^W\boldsymbol{\omega}_{C_{k-1}}]_\times^2\,{}^WR_{C_{k-1}}\,{}^{O_{k-1}}\boldsymbol{p}_{C_k}(\boldsymbol{q}_j) \\ &+ 2[{}^W\boldsymbol{\omega}_{C_{k-1}}]_\times\,{}^WR_{C_{k-1}}\,{}^{O_{k-1}}\dot{\boldsymbol{p}}_{C_k}(\boldsymbol{q}_j, \boldsymbol{\alpha}_j)\Big] \end{aligned} \tag{14}$$

Notice that ${}^W\dot{\boldsymbol{\omega}}_{C_i}$, a function of $\dot{\boldsymbol{x}}$, appears in these formulas. From (11) and (13), we write the accelerometer output as follows

$$\boldsymbol{y}_a = \widetilde{h}(\boldsymbol{x}, \dot{\boldsymbol{x}}, \boldsymbol{u}) \tag{15}$$

To remove the dependency of h in $\dot{\boldsymbol{x}}$, we use the state dynamics (10). Thus, from (10), (12) and (15), we get the sensor dynamics equation, in the desired form (5)

$$\begin{pmatrix} \boldsymbol{y}_g \\ \boldsymbol{y}_a \end{pmatrix} = h(\boldsymbol{x}, \boldsymbol{u}) \tag{16}$$

IV. Proof of observability

Using (10) and (16), we now prove Theorem 1. Let $\boldsymbol{u}$ be any input of the system: we show that, using the state and sensor dynamics, the measurements uniquely determine $\boldsymbol{x}$.

From (12) and its time derivative, we get

$$\begin{cases} {}^{C_i}R_W\,{}^W\boldsymbol{\omega}_{C_i} = {}^{C_i}R_{I_i}(\boldsymbol{q}_j)\boldsymbol{y}_g - {}^{C_i}\boldsymbol{\omega}_{I_i}(\boldsymbol{q}_j, \boldsymbol{\alpha}_j) \\ {}^{C_i}R_W\,{}^W\dot{\boldsymbol{\omega}}_{C_i} = \dfrac{d}{dt}\left({}^{C_i}R_{I_i}(\boldsymbol{q}_j)\boldsymbol{y}_g - {}^{C_i}\boldsymbol{\omega}_{I_i}(\boldsymbol{q}_j, \boldsymbol{\alpha}_j)\right) \end{cases} \tag{17}$$

According to (2), the right hand sides of these equations only depend on $\boldsymbol{u}$, $\boldsymbol{y}_g$ and its derivative $\dot{\boldsymbol{y}}_g$, and is thus entirely known. Thus, ${}^{C_i}R_W\,{}^W\boldsymbol{\omega}_{C_i}$ and ${}^{C_i}R_W\,{}^W\dot{\boldsymbol{\omega}}_{C_i}$ may be computed: physically, this reflects the fact that, subtracting the rigid kinematics from the gyroscope readings, one can infer the angular velocity and angular acceleration of the set S_i in the body frame C_i without any ambiguity.

Similarly, using the fact that for any rotation R

$$\forall \boldsymbol{a}, \boldsymbol{b} : [R\boldsymbol{a}]_\times \boldsymbol{b} = R[\boldsymbol{a}]_\times R^T\boldsymbol{b} \tag{18}$$

and by substituting (13) into (15), the latter can be rewritten as follows

$$\begin{aligned} {}^{C_i}R_W({}^W\ddot{\boldsymbol{p}}_{O_i} - {}^W\boldsymbol{g}) = {}&{}^{C_i}R_{I_i}(\boldsymbol{q}_j)\boldsymbol{y}_a \\ &- {}^{C_i}\ddot{\boldsymbol{p}}_{a_i}(\boldsymbol{q}_j, \boldsymbol{\alpha}_j, \dot{\boldsymbol{\alpha}}_j) \\ &+ [{}^{C_i}R_W\,{}^W\dot{\boldsymbol{\omega}}_{C_i}]_\times\,{}^{C_i}\boldsymbol{p}_{a_i}(\boldsymbol{q}_j) \\ &+ [{}^{C_i}R_W\,{}^W\boldsymbol{\omega}_{C_i}]_\times^2\,{}^{C_i}\boldsymbol{p}_{a_i}(\boldsymbol{q}_j) \\ &+ 2[{}^{C_i}R_W\,{}^W\boldsymbol{\omega}_{C_i}]_\times\,{}^{C_i}\dot{\boldsymbol{p}}_{a_i}(\boldsymbol{q}_j, \boldsymbol{\alpha}_j) \end{aligned} \tag{19}$$

From these quantities, we now compute the orientation matrices ${}^{C_i}R_W$, and the corresponding angular velocity. For this, we use the system dynamics (10). However, instead of using the algebraic value of the matrices in (10), we reformulate these dynamics using Newton and Euler's laws of motion. Consider the set S_i. This set is subjected to three external actions: gravity, the force and torque due to the link with S_{i-1}, and those due to the link with S_{i+1}. Note ${}^W\boldsymbol{F}_i$ the force exerted on S_i by S_{i-1}, expressed in the world frame. The torque applied at this point, $\boldsymbol{\tau}_i$, is defined by (1), in frame C_i. By convention, we have ${}^W\boldsymbol{F}_{n+1} = 0$ and $\boldsymbol{\tau}_{n+1} = 0$, as S_n is the last set of the open kinematic chain. Writing Newton's law of motion for set S_i in the world frame gives:

$$m_i\,{}^W\ddot{\boldsymbol{p}}_{G_i} = m_i\,{}^W\boldsymbol{g} + {}^W\boldsymbol{F}_i - {}^W\boldsymbol{F}_{i+1} \tag{20}$$

where m_i is the mass of the set S_i, and G_i its center of mass. Writing (20) for $i = 1, .., n$ and solving the $n \times n$ linear system of equations for the forces yields

$$\forall i \in [1, n] : {}^W\boldsymbol{F}_i = \sum_{k=i}^{n} m_k({}^W\ddot{\boldsymbol{p}}_{G_k} - {}^W\boldsymbol{g}) \tag{21}$$

We now apply Euler's law of motion at point O_i to the set S_i, along the world frame axes. As O_i is not fixed in W, we add the torque due to the inertia forces related to the translational motion of O_i with respect to the world. Writing $\boldsymbol{L}(S_i)$ the angular momentum of the set S_i with respect to O_i, in W, this gives

$$\begin{aligned} \frac{d}{dt}\big(\boldsymbol{L}(S_i)\big) = {}&m_i[{}^WR_{C_i}\,{}^{C_i}\boldsymbol{p}_{G_i}(\boldsymbol{q}_j)]_\times({}^W\boldsymbol{g} - {}^W\ddot{\boldsymbol{p}}_{O_i}) \\ &+ [{}^WR_{C_i}\,{}^{C_i}\boldsymbol{p}_{O_{i+1}}(\boldsymbol{q}_j)]_\times\,{}^W\boldsymbol{F}_{i+1} \\ &+ {}^WR_{C_i}\boldsymbol{\tau}_i \\ &- {}^WR_{C_{i+1}}\boldsymbol{\tau}_{i+1} \end{aligned} \tag{22}$$

Isolating the last two terms, we rewrite this equation according to the following property:

Lemma 1: Let $Z_i = (\boldsymbol{y}_a, \boldsymbol{y}_g, \dot{\boldsymbol{y}}_g, \boldsymbol{u}, {}^{C_{i+1}}R_{C_i}, ..., {}^{C_n}R_{C_{n-1}})$. There exists a function Φ_i of Z_i, expressed in Appendix, such that:

$$\boldsymbol{\tau}_i = {}^{C_i}R_{C_{i+1}}\boldsymbol{\tau}_{i+1} + \Phi_i(Z_i) \tag{23}$$

The constructive proof is given in Appendix. The important feature in (23) is its triangular structure, where $\boldsymbol{\tau}_i$ is expressed as a function of sensor data and of downstream deformations only. This naturally leads to a proof by induction initialized at the last joint of the kinematic chain: writing (23) for the last set, $i = n$, since $\boldsymbol{\tau}_{n+1} = 0$ and Z_n contains only sensor data, $\boldsymbol{\tau}_n$ is known, and, from (1), ${}^{C_{n-1}}R_{C_n}$, is known. Recursively, all the rotation matrices ${}^{W}R_{C_i}$ are uniquely determined by successive reconstruction of ${}^{C_{i-1}}\boldsymbol{\Omega}_{C_i}$. Then from (17), we compute ${}^{W}\boldsymbol{\omega}_{C_i}$, and thus the full state $\boldsymbol{x}$. This concludes the proof.

V. Implementation and Results

The preceding study of observability suggests that a state-of-the-art observer should produce satisfactory results. In this section, we present a simulation study of an Extended Kalman Filter (EKF) based on (10) and (16). Although the observability property does not guarantee the convergence of the EKF, the EKF is a natural first choice for implementation of an asymptotic observer, as illustrated in several contributions in the literature [13] [15]. Moreover, the implementation of the EKF is made particularly convenient by the combined use of the open-source generic implementation of such observer by LAAS [21], and the open-source dynamics library Pinocchio [22], which is used to implement (10). The resulting observer is tested, first on a simulation model, then on real data from the robotic platform depicted in Figure 1.

A. Simulation on a triple inverted pendulum

Consider the case of a robot arm with compliant joints. A usual task for such a robot is to control the position of the tip of the arm. However, due to the compliance, rigid computation of the robot kinematics does not give the correct position, and thus cannot track the target trajectory.

Here, we consider as a simplification a triple, actuated, inverted pendulum, such as described by Figure 3 and Table II. The pendulum has three arms, the first and third rotating around their local X axis, and the second around its local Y axis. The arms are weightless, and a point mass is present at the tip of each pendulum. We consider each joint to be flexible, with the given model of (1) - the stiffness matrix is taken proportional to identity. However, to introduce some realism into the simulation, a viscous damping term is added to the simulation model. In accordance with the methodology advocated and studied in this article, one IMU is placed at the midpoint of each arm, at a_1, a_2 and a_3 respectively.

TABLE II
Parameters used for the simulation.

Length (m)		Mass (kg)		Stiffness (Nm.rad^{-1})		Damping (Nm.s.rad^{-1})	
L_1	1	m_1	1	K_1	800	ν_1	8
L_2	0.5	m_2	1	K_2	400	ν_2	4
L_3	0.5	m_3	1	K_3	150	ν_3	1.5

In simulation, a sinusoidal motion of the rigid joints is generated, giving a closed trajectory for the tip of the arm (as all frequencies are taken equal). However, this motion generates oscillations of the flexible joints, leading to an error in position of the tip of the arm (see Figure 4). We use the designed observer to reconstruct this position. To model sensor inaccuracy, a white noise is added, of standard deviation 0.2 m.s^{-2} and 0.015 rad.s^{-1} respectively

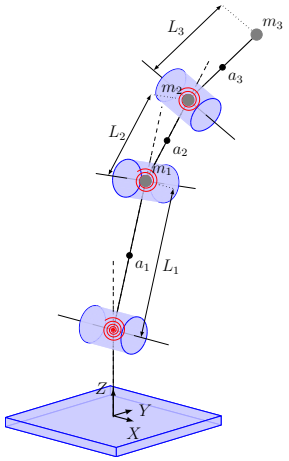

Fig. 3. Kinematics of the simulated system.

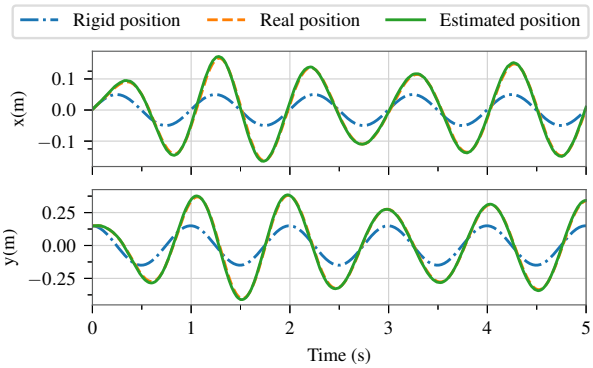

Fig. 4. Simulation results: position of the tip of the pendulum, as given by the rigid and flexible model, and EKF estimation.

to the accelerometer and gyroscope. A constant bias of norm 0.4 m.s^{-2} and 0.03 rad.s^{-1} is also added to some axis of each sensor. These values are consistent with the off-the-shelves sensors being used on Wandercraft exoskeleton. Finally, the presence of viscous damping in the simulation, which is not taken into account by the observer, is another source of error. Figure 4 shows the resulting tip trajectory, for the rigid and flexible case, and for the observer. Despite imperfect sensors and modeling discrepancies, the observer manages to estimate the real trajectory of the tip, with the observed tip trajectory remaining less than 1 cm from the real trajectory, out of an average error of 13.5 cm for the rigid model. This error largely comes from adding damping to the dynamics: indeed, as a sensitivity study reveals it, the bias added to the sensor account for only 1 mm of error on average. Thus, the proposed observer reveals quite robust to sensor additive bias.

B. Experiment on an exoskeleton

Wandercraft develops Atalante™ (see Figure 1 (left)), an exoskeleton designed to enable paraplegic patients to stand up, and walk without any external assistance. The exoskeleton reproduces the kinematics of the human lower limbs. However, the structure is not fully rigid, and, under its own weight added to that of the patient, undergoes deformations (see Figure 1 (right)). Analysis with a motion capture device from OptiTrack has shown that while the structural parts like the tibia or the thigh remain rigid, small deformations are observed around each joint of the system.

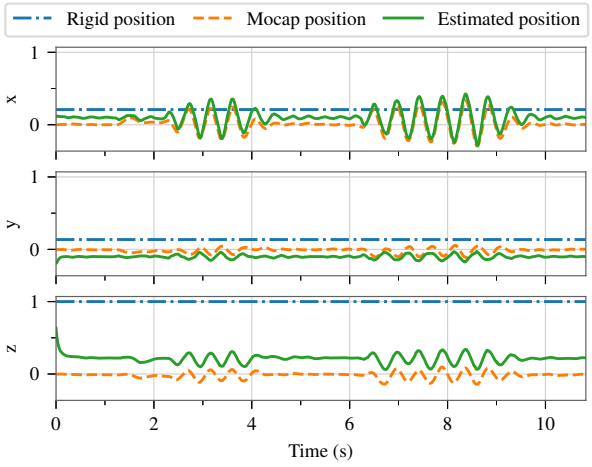

Fig. 5. Experimental results: position of the flying foot, given by the rigid model, the motion capture and the observer. Data is normalized using the initial error on the z axis.

The main deformations happen at the support ankle and the hips, thus, for design simplicity, we consider only these three deformations, and place three IMUs, one in each leg and one in the back. Their position and orientation are known from the blueprint of the device. Thus, this setup satisfies assumptions 2 - 3. Note that these IMUs are mass-market MEMS components, thus characterized by a high level of noise and bias, as mentioned in the previous section.

In the experiment presented in Figure 5, the robot is standing on one leg, with a foot in the air, as shown in Figure 1. Manually, the foot is pushed, leading to deformations and foot oscillations. The proposed EKF is then run (offline) on data from this experiment. This observer requires the robot kinematics (joint and flexibility position), mass and inertia: this data is extracted from the robot CAD design. The stiffness associated to each flexibility is identified by trial and error procedure, to minimize the observer error in term of flying foot and center of mass position, during the oscillatory phase. Finally, the observer is fed with the position, velocity and acceleration of the robot joints, measured by rotary encoders, and the IMU signals. Figure 5 reports the result of this experiment. As expected, the rigid computation of the position remains constant, stressing that no encoder motion was present. On the contrary, the observer gives an estimate much closer to the actual value, and captures the dynamic behavior of the foot as it is pushed. Indeed, during the oscillation phase, the remaining error has an amplitude 3.5 times smaller thanks to the observer.

There remains however a constant bias, accounting for about 25% of the total deformation. As seen in simulations, sensor bias do not explain such an error : indeed, computing them offline and removing them changes only slightly the results. Instead, this bias is probably due to model inaccuracies, at least at three levels. First, the proposed kinematics having three deformations in an otherwise rigid exoskeleton is only an approximation. The motion capture indeed shows small deformations at other points: if one reconstructs the position of the flying foot from the motion capture angular deformation, taking into account only the three identified deformations, one finds a similar level of error to that of the observer. Second, modeling the dynamics of the flexibilites by a linear spring of constant stiffness is also debatable. In practice it is highly unlikely that the deformation is linear with the applied torque. Mechanical backlash may also explain part of this deformation, which is not taken into account by this model. In fact, the tuning of the joint stiffness for the observer differs depending on the rigid configuration. An average constant stiffness is chosen, but while it keeps giving a better estimate of the position of the flying foot than the rigid model, its performance will most likely decrease in some configurations. This is in our opinion the main limitation of the proposed approach. Future contributions may include a more advanced model of the deformations, e.g. featuring backlash. Importantly, a static bias such as the one observed in Figure 5 can be reproduced in simulations by simply adding a constant bias to the stiffness matrix. Third, while we assumed the pose of the IMUs known, on the real robot there is an additional uncertainty on the orientation of the IMUs in the body frame, which, in turn, impacts the definition of ${}^{W}R_{I}$ in Equation (11).

VI. Conclusion

In this paper, we have presented a methodology for estimating several deformations of an articulated set of rigid bodies. Assuming these deformations are punctual rotations, behaving like a spring, we have shown that, by placing one IMU between each deformation, the system is fully observable. An Extended Kalman Filter has been used as state observer and has been tested, both in simulation and on a real platform. Simulation show that this observer is quite robust to sensor bias. The observer was run on experimental data from an exoskeleton, where it gives a good estimate of the position of the flying foot, despite kinematic and dynamic modeling error introducing bias. This information may now be used in future works to control the real position of the flying foot, during a walking motion. The performance of this observer may also be improved further. The chosen kinematic model of three deformations might be refined, to better capture the error in foot position seen by the motion capture. The dynamic model of a linear spring of constant stiffness might also be revised, to capture the change of stiffness as the robot moves. Finally, the observer design could be expanded to a walking scenario, where changes in the number of contacts would modify the dynamics of the system. In that context, the dependence of our observer on articular acceleration poses new exciting challenges.

References

[1] F. Lewis, D. Dawson, and C. Abdallah, *Robot Manipulator Control: Theory and Practice*, 2nd ed. New York: Marcel Dekker, 2004. [Online]. Available: https://www.crcpress.com/Robot-Manipulator-Control-Theory-and-Practice/Lewis-Dawson-Abdallah/p/book/9780824740726

[2] H. G. Sage, M. F. D. Mathelin, and E. Ostertag, "Robust control of robot manipulators: A survey," *International Journal of Control*, vol. 72, no. 16, pp. 1498–1522, Jan. 1999. [Online]. Available: https://doi.org/10.1080/002071799220137

[3] E. Garcia, M. A. Jimenez, P. G. D. Santos, and M. Armada, "The evolution of robotics research," *IEEE Robotics Automation Magazine*, vol. 14, no. 1, pp. 90–103, Mar. 2007.

[4] J. W. Grizzle, C. Chevallereau, R. W. Sinnet, and A. D. Ames, "Models, feedback control, and open problems of 3d bipedal robotic walking," *Automatica*, vol. 50, no. 8, pp. 1955–1988, Aug. 2014. [Online]. Available: http://www.sciencedirect.com/science/article/pii/S0005109814001654

[5] T. A. McMahon, "The role of compliance in mammalian running gaits," *The Journal of Experimental Biology*, vol. 115, pp. 263–282, Mar. 1985.

[6] T. Hamel and R. Mahony, "Attitude estimation on SO[3] based on direct inertial measurements." IEEE, 2006, pp. 2170–2175.

[7] R. Mahony, T. Hamel, and J. Pflimlin, "Nonlinear Complementary Filters on the Special Orthogonal Group," *IEEE Transactions on Automatic Control*, vol. 53, no. 5, pp. 1203–1217, Jun. 2008.
[8] T. Michel, P. Genevs, H. Fourati, and N. Layada, "On Attitude Estimation with Smartphones," Mar. 2017.
[9] J. L. Crassidis, F. L. Markley, and Y. Cheng, "Survey of Nonlinear Attitude Estimation Methods," *Journal of Guidance, Control, and Dynamics*, vol. 30, no. 1, pp. 12–28, 2007.
[10] S. Trimpe and R. D'Andrea, "Accelerometer-based tilt estimation of a rigid body with only rotational degrees of freedom," in *2010 IEEE International Conference on Robotics and Automation*, May 2010, pp. 2630–2636.
[11] P. Cheng and B. Oelmann, "Joint-Angle Measurement Using Accelerometers and Gyroscopes: A Survey," *IEEE Transactions on Instrumentation and Measurement*, vol. 59, no. 2, pp. 404–414, Feb. 2010.
[12] P. Pierro, P. C. A. Monje, P. N. Mansard, P. P. Soures, and P. C. Balaguer, "Open Solution for Humanoid Attitude Estimation through Sensory Integration and Extended Kalman Filtering," *Automatika*, vol. 56, no. 1, pp. 9–20, Jan. 2015. [Online]. Available: https://www.tandfonline.com/doi/abs/10.7305/automatika.2015.04.593
[13] S. Khandelwal and C. Chevallereau, "Estimation of the Trunk Attitude of a Humanoid by Data Fusion of Inertial Sensors and Joint Encoders," in *Nature-Inspired Mobile Robotics*. Singapour: World Scientific, 2013, pp. 822–830.
[14] N. Roy, P. Newman, and S. Srinivasa, "State Estimation for Legged Robots: Consistent Fusion of Leg Kinematics and IMU," in *Robotics:Science and Systems VIII*. MIT Press, 2013, pp. 504–. [Online]. Available: http://ieeexplore.ieee.org/xpl/articleDetails.jsp?arnumber=6577984
[15] M. Benallegue and F. Lamiraux, "Estimation and Stabilization of Humanoid Flexibility Deformation Using Only Inertial Measurement Units and Contact Information," *International Journal of Humanoid Robotics*, vol. 12, no. 3, Sep. 2015.
[16] T. Flayols, A. Del Prete, P. Wensing, A. Mifsud, M. Benallegue, and O. Stasse, "Experimental evaluation of simple estimators for humanoid robots," in *2017 IEEE-RAS 17th International Conference on Humanoid Robotics (Humanoids)*, Nov. 2017, pp. 889–895.
[17] A. Mifsud, M. Benallegue, and F. Lamiraux, "Estimation of contact forces and floating base kinematics of a humanoid robot using only Inertial Measurement Units," in *2015 IEEE/RSJ International Conference on Intelligent Robots and Systems (IROS)*, Sep. 2015, pp. 3374–3379.
[18] J. Stuelpnagel, "On the Parametrization of the Three-Dimensional Rotation Group," *SIAM Review*, vol. 6, no. 4, pp. 422–430, Oct. 1964. [Online]. Available: https://epubs.siam.org/doi/abs/10.1137/1006093
[19] R. Featherstone, *Rigid Body Dynamics Algorithms*. Springer US, 2008.
[20] G. Besançon, *Nonlinear Observers and Applications*, ser. Lecture Notes in Control and Information Sciences. Berlin Heidelberg: Springer-Verlag, 2007.
[21] M. Benallegue, A. Mifsud *et al.*, "state-observation: interfaces for state observers, including linear and extended kalman filters." https://github.com/stack-of-tasks/state-observation, 2015–2018.
[22] J. Carpentier, F. Valenza, N. Mansard *et al.*, "Pinocchio: fast forward and inverse dynamics for poly-articulated systems," https://stack-of-tasks.github.io/pinocchio, 2015–2018.

APPENDIX

Proof of Lemma 1:

Let us define the following quantities

$$\begin{cases} \Phi_{i,1} = {}^{C_i}R_W \dfrac{d}{dt}\big(\boldsymbol{L}(S_i)\big) \\ \Phi_{i,2} = {}^{C_i}R_W[{}^W R_{C_i}\, {}^{C_i}\boldsymbol{p}_{G_i}(\boldsymbol{q}_j)]_\times ({}^W\boldsymbol{g} - {}^W\ddot{\boldsymbol{p}}_{O_i}) \\ \Phi_{i,3} = {}^{C_i}R_W[{}^W R_{C_i}\, {}^{C_i}\boldsymbol{p}_{O_{i+1}}(\boldsymbol{q}_j)]_\times {}^W\boldsymbol{F}_{i+1} \end{cases} \tag{24}$$

Using (22) in (23) defines Φ_i as

$$\Phi_i(Z_i) = \Phi_{i,1} + \Phi_{i,2} + \Phi_{i,3} \tag{25}$$

Thus, to prove Lemma 1, we show that each $\Phi_{i,j}$ depends on Z_i only.

To compute the angular momentum of the set S_i, $\boldsymbol{L}(S_i)$, we once again decompose the motion of the bodies of S_i as their motion inside C_i, due to rigid motion, and their motion due to the deformation, i.e. the rotation of C_i. Calling $\boldsymbol{L}(S_i/C_i)$ the angular momentum of these bodies relative to O_i due to the rigid motion, in C_i (which depends only on $\boldsymbol{q}_j$ and $\boldsymbol{\alpha}_j$), we have:

$$\begin{aligned} \boldsymbol{L}(S_i) = {}&{}^W R_{C_i}\boldsymbol{L}(S_i/C_i)(\boldsymbol{q}_j, \boldsymbol{\alpha}_j) \\ &+ \sum_{l=1}^{n_i} {}^W R_{C_i}\, {}^{C_i}I_{i,l}(\boldsymbol{q}_j)\, {}^{C_i}R_W\, {}^W\boldsymbol{\omega}_{C_i} \\ &- \sum_{l=1}^{n_i} m_{i,l}[{}^W R_{C_i}\, {}^{C_i}\boldsymbol{p}_{i,l}(\boldsymbol{q}_j)]^2_\times\, {}^W\boldsymbol{\omega}_{C_i} \end{aligned} \tag{26}$$

where n_i is the number of bodies of S_i, and, for l in $[1, n_i]$, $m_{i,l}$, ${}^{C_i}I_{i,l}$ and ${}^{C_i}\boldsymbol{p}_{i,l}$ are respectively the mass, inertia (expressed at O_i in C_i) and position of the center of mass of the lth body of S_i.

Using (18), (26) become:

$$\boldsymbol{L}(S_i) = {}^W R_{C_i}\boldsymbol{\mu}_i \tag{27}$$

with:

$$\begin{aligned} \boldsymbol{\mu}_i = {}&\boldsymbol{L}(S_i/C_i)(\boldsymbol{q}_j, \boldsymbol{\alpha}_j) \\ &+ \sum_{l=0}^{n_i} {}^{C_i}I_{i,l}(\boldsymbol{q}_j)\, {}^{C_i}R_W\, {}^W\boldsymbol{\omega}_{C_i} \\ &- \sum_{l=0}^{n_i} m_{i,l}[{}^{C_i}\boldsymbol{p}_{i,l}(\boldsymbol{q}_j)]^2_\times\, {}^{C_i}R_W\, {}^W\boldsymbol{\omega}_{C_i} \end{aligned} \tag{28}$$

From (17), we get that $\boldsymbol{\mu}_i$ is function of $\boldsymbol{q}_j$, $\boldsymbol{\alpha}_j$ and $\boldsymbol{y}_g$ only.

Derivating (27), we get:

$$\Phi_{i,1} = [{}^{C_i}R_W\, {}^W\boldsymbol{\omega}_{C_i}]_\times \boldsymbol{\mu}_i + \frac{d}{dt}\boldsymbol{\mu}_i \tag{29}$$

Once again using (17), (29) shows that $\Phi_{i,1}$ is a function of Z_i.

Using (18) on (24) directly yields

$$\Phi_{i,2} = [{}^{C_i}\boldsymbol{p}_{G_i}(\boldsymbol{q}_j)]_\times\, {}^{C_i}R_W({}^W\boldsymbol{g} - {}^W\ddot{\boldsymbol{p}}_{O_i}) \tag{30}$$

which, from (19), is indeed a function of Z_i.

Finally, using (18) on (24) yields

$$\Phi_{i,3} = [{}^{C_i}\boldsymbol{p}_{O_{i+1}}(\boldsymbol{q}_j)]_\times\, {}^{C_i}\boldsymbol{F}_{i+1} \tag{31}$$

For $i = n$, ${}^W\boldsymbol{F}_{i+1} = 0$ and the property is trivial. Otherwise, using (21) to get the value of the force, and expressing ${}^W\ddot{\boldsymbol{p}}_{G_k}$ in terms of ${}^W\ddot{\boldsymbol{p}}_{O_i}$ yields

$$\begin{aligned} {}^{C_i}\boldsymbol{F}_{i+1} = {}&{}^{C_i}R_W \sum_{j=i+1}^{n} m_j({}^W\ddot{\boldsymbol{p}}_{G_j} - {}^W\boldsymbol{g}) \\ = {}&\sum_{j=i+1}^{n} m_j\, {}^{C_i}R_{C_j}\Big[{}^{C_j}R_W({}^W\ddot{\boldsymbol{p}}_{O_j} - {}^W\boldsymbol{g}) \\ &+ {}^{C_j}\ddot{\boldsymbol{p}}_{G_j}(\boldsymbol{q}_j, \boldsymbol{\alpha}_j, \dot{\boldsymbol{\alpha}}_j) \\ &+ [{}^{C_j}R_W\, {}^W\dot{\boldsymbol{\omega}}_{C_j}]_\times\, {}^{C_j}\boldsymbol{p}_{G_j}(\boldsymbol{q}_j) \\ &+ [{}^{C_j}R_W\, {}^W\boldsymbol{\omega}_{C_j}]^2_\times\, {}^{C_j}\boldsymbol{p}_{G_j}(\boldsymbol{q}_j) \\ &+ 2[{}^{C_j}R_W\, {}^W\boldsymbol{\omega}_{C_j}]_\times\, {}^{C_j}\dot{\boldsymbol{p}}_{G_j}(\boldsymbol{q}_j, \boldsymbol{\alpha}_j)\Big] \end{aligned} \tag{32}$$

The whole term in brackets, using again (17) and (19), depends on $\boldsymbol{u}$, $\boldsymbol{y}_g$, $\dot{\boldsymbol{y}}_g$ and $\boldsymbol{y}_a$. Thus, F_{i+1} depends on these variables, as well as on ${}^{C_i}R_{C_j}$ for $j > i$, making it a function of Z_i. This ends the proof.